

Coulomb and nuclear breakup of ^8B

R. Shyam^{a*} and I.J. Thompson^{b†}

^a*Saha Institute of Nuclear Physics, Calcutta - 700 064, India*

^b*Department of Physics, University of Surrey, Guildford GU2 5XH, U.K.*

Abstract

The cross sections for the ($^8\text{B}, ^7\text{Be-p}$) breakup reaction on ^{58}Ni and ^{208}Pb targets at the beam energies of 25.8 MeV and 415 MeV have been calculated within a one-step prior-form distorted-wave Born approximation. The relative contributions of Coulomb and nuclear breakup of $E1$ and $E2$ multipolarities as well as their interference have been determined. The nuclear breakup contributions are found to be substantial in the angular distributions of the ^7Be fragment for angles in the range of $30^\circ - 80^\circ$ at 25.8 MeV beam energy. The Coulomb-nuclear interference terms make the $E1$ cross section larger than that of $E2$ even at this low beam energy. However, at the incident energy of 415 MeV, these effects are almost negligible in the angular distributions of the ($^7\text{Be-p}$) coincidence cross sections at angles below 4° .

KEYWORDS: Coulomb and nuclear breakup of ^8B , prior-form DWBA theory, $E1$ and $E2$ breakup cross sections, nuclear breakup effects.

PACS NO. 25.70.De, 25.40.Lw, 96.60.Kx

*E-mail address: shyam@tnp.saha.ernet.in

†E-mail address: I.Thompson@surrey.ac.uk

1 Introduction

The Coulomb dissociation (CD) method provides an alternate indirect way to determine the cross sections for the radiative capture reaction ${}^7\text{Be}(p, \gamma){}^8\text{B}$ at low relative energies [1, 2], which is the most important and most uncertain nuclear input to the standard solar model calculations [3, 4]. The CD method reverses the radiative capture by the dissociation of a projectile (the fused system) in the Coulomb field of a target by making the assumption that nuclei do not interact strongly and the electromagnetic excitation process is dominated by a single multipolarity.

Motobayashi et al. performed the first measurement of the breakup of ${}^8\text{B}$ into ${}^7\text{Be}$ - p low energy continuum in the field of ${}^{208}\text{Pb}$ with a radioactive ${}^8\text{B}$ beam of 46.5 MeV/A energy [5], which was analyzed by us [6] using Alder-Winther's semiclassical theory of Coulomb excitation (which assumes the colliding nuclei are point-like objects) [7]. Considering only the $E1$ component of the excitation, the measured breakup cross sections were found to be consistent with a $S_{17}(0) = (15.5 \pm 2.80)$ eV barn. However, in the CD of ${}^8\text{B}$ at these energies, the $E2$ component of breakup may not be negligible [8], and its presence affects the extracted $S_{17}(0)$ [6]. Thus, a reliable estimate of this component is necessary for the accurate extraction of the astrophysical S-factor ($S_{17}(0)$) from the breakup data.

Since the contribution of the $E2$ component is strongly dependent on the nuclear structure model of ${}^8\text{B}$ (which is not yet known with certainty), the RIKEN group has repeated the breakup measurements with angular distributions extended to larger scattering angles where the cross sections are more sensitive to the $E2$ component [9]. An analysis of this data within the distorted wave Born-approximation (where the breakup is treated as the inelastic excitation of the projectile to the continuum) led these authors to conclude that the $E2$ components and the nuclear breakup effects are considerably smaller. However, they use a collective model prescription to calculate the inelastic nuclear form factor (see eg. [6]). Due to a long tail in the ${}^8\text{B}$ g.s wave function this procedure is unlikely to be accurate. Furthermore, Coulomb breakup is calculated by a point projectile and target approximation (PLPTA) in these studies, and its range of validity is yet to be determined for this projectile.

The Notre Dame group has measured the breakup of ${}^8\text{B}$ on the ${}^{58}\text{Ni}$ target at the beam energy of 25.8 MeV, well below the Coulomb barrier, where the $E2$ component is expected to dominate the CD process [10]. However, the reliable extraction of the $E2$ component from this data, where only the the integrated cross section of the ${}^7\text{Be}$ fragment is measured, is still doubtful. The analysis of the data reported in Ref. [10] used the Alder-Winther's semiclassical theory of Coulomb excitation, where the final state is treated as a two-body system, thus assuming that the measured angles of ${}^7\text{Be}$ were equal to those of the ${}^7\text{Be}$ -

p center of mass. The inadequacy of this assumption has been demonstrated in [11]. Furthermore, the total breakup cross section reported in this experiment could not be reproduced within the Alder-Winther theory even if a wide variety of structure models of ${}^8\text{B}$ were used [12]. On the other hand, the importance of the nuclear breakup effects in the kinematical regime of this experiment has recently been emphasized [13]. Therefore, there is a need to reanalyze this data using a proper theory where Coulomb and nuclear breakup effects are included on the equal footing and the three-body kinematics is taken into account.

In this paper we perform a one-step prior-form DWBA analysis of the ${}^8\text{B}$ breakup data at both low and high energies in order to check the validity of various assumptions of the Coulomb dissociation method. We describe the breakup process as a single proton excitation of the projectile from its ground state to a range of states in the continuum, which is discretized by the method of continuum bins.

In previous calculations [12, 13] based on this model, quadrupole transitions from the ground state to the continuum did not include the excitation of f partial waves. Moreover, the numerical calculations were performed only for the breakup reaction ${}^8\text{B} + {}^{58}\text{Ni} \rightarrow {}^7\text{Be} + X$ at the beam energy of 25.8 MeV where the final state was considered as a two-body system. In this work we improve upon this aspect by using a proper three-body kinematics for the final state, and also include excitations of $\ell = 3$ continuum states. We furthermore apply our model to the RIKEN data where ${}^7\text{Be}$ and p were detected in coincidence with very small relative energies in a ${}^8\text{B}$ induced reaction on ${}^{208}\text{Pb}$ target at the beam energy of 415 MeV. We avoid the point-like projectile approximation as well as collective model prescription for the nuclear form factor, by determining the nuclear and Coulomb parts by a single-folding method where the relevant fragment-target interactions are folded by the projectile wave functions in the ground and continuum states.

We present our formalism in the next sections. Details of the numerical calculations are described in section 3. The results of our calculations and their discussions are presented in section 4, while the summary and conclusions of our work are given in section 5.

2 Formalism

2.1 Coincidence cross sections

The triple differential cross section for the breakup of a projectile (a) into its fragments (b and x), $A + a \rightarrow b + x + A$, can be related to the inelastic excitation

of the projectile a to its continuum, $A + a \rightarrow a^* + A$ as ([11])

$$\frac{d\sigma}{dE_b d\Omega_b d\Omega_x} = \frac{J}{4\pi} \frac{d\sigma}{dE_{bx} d\Omega_{a^*}} \frac{\partial E_x}{\partial E_{tot}}, \quad (1)$$

where the total kinetic energy

$$\begin{aligned} E_{tot} &= E_b + E_x + E_A \\ &= E_{bx} + E_{a^*} + \frac{P^2}{2(m_a + m_A)}. \end{aligned} \quad (2)$$

is related to the projectile energy (E_p) and the reaction Q-value (Q) by $E_{tot} = E_p + Q$. In Eq. (2) E_b , E_x , and E_A are the kinetic energies of the fragments b , x and recoiling target nucleus respectively, while E_{bx} and E_{a^*} are the kinetic energies of the relative motion of the fragments and of their CM with respect to the target nucleus respectively. In Eq. (1), we have assumed that the angular distribution of fragments is isotropic in the projectile rest frame; the expressions without making this assumption are given in Ref. [14]. The last factor in Eq. (1) is given by

$$\frac{\partial E_x}{\partial E_{tot}} = m_A [m_x + m_A - m_x \frac{\mathbf{p}_x \cdot (\mathbf{P} - \mathbf{p}_b)}{p_x^2}]^{-1}, \quad (3)$$

and the Jacobian J is defined as

$$J = \frac{m_b p_b m_x p_x}{\mu_{bx} p_{bx} \mu_{aA} p_{a^*}}. \quad (4)$$

In Eq. (3)-(4), m_i is the mass of the fragment i , and μ_{aA} and μ_{bx} are the reduced masses of the $a - A$ and $b - x$ systems respectively. \mathbf{P} is the total momentum which is fixed by the conditions in the entrance channel. The momenta \mathbf{p}_{bx} and \mathbf{p}_{a^*} describing the relative motion of the fragments b and x and the motion of their CM with respect to the target nucleus respectively, can be related to their individual momenta \mathbf{p}_b and \mathbf{p}_x by straight-forward expressions (see. e.g. Ref. [15, 11]). $d\sigma/dE_{bx} d\Omega_{a^*}$ describes the inelastic excitation of the projectile from its ground state to the state \mathbf{k}_{bx} in the continuum.

The coordinates \mathbf{R} and \mathbf{r} describing the motion of the CM of the fragments with respect to the target and their relative motion respectively are related to those of the relative motion of the individual fragments from the target (\mathbf{r}_x and \mathbf{r}_b) by

$$\begin{aligned} \mathbf{r}_x &= \mathbf{R} + \frac{m_b}{m_a} \mathbf{r}, \\ \mathbf{r}_b &= \mathbf{R} + \frac{m_x}{m_a} \mathbf{r}. \end{aligned} \quad (5)$$

2.2 Final state wave function

In general, all states, including the ground state ϕ_0 , and excited continuum states $\phi_{k_{bx}}$, are coupled together due to interactions $V_{bA}(\mathbf{r}_b)$ and $V_{xA}(\mathbf{r}_x)$. The wave

function $\Psi_{j_f}^{M_f}$ at some given energy of the final channel is given by

$$\begin{aligned} \Psi_{J_f}^{M_f}(\mathbf{R}, \mathbf{r}) &= \sum_{L_f J_p, \mathbf{k}_{bx}, M_f \mu_p} \phi_{J_p \mu_p, \mathbf{k}_{bx}}(\mathbf{r}) \langle L_f M_f J_p \mu_p | J_f M_f \rangle i^{L_f} Y_{L_f}^{M_f}(\hat{\mathbf{R}}) \\ &\times \frac{1}{R} f_{L_f, J_p, \mathbf{k}_{bx}}^{J_f}(R) \end{aligned} \quad (6)$$

In the following the set $\{L_f, J_p, \mathbf{k}_{bx}; J\}$ will be abbreviated as α .

The breakup couplings to be defined later will lead to the usual set of coupled equations for the wave function f_α .

$$\left[-\frac{\hbar^2}{2\mu} \left(\frac{d^2}{dR^2} - \frac{L(L+1)}{R^2} \right) + E_{bx} - E \right] f_\alpha(R) + \sum_{\alpha'} i^{L'-L} U_{\alpha; \alpha'}(R) f_{\alpha'}(R) = 0, \quad (7)$$

where E_{bx} is the energy associated with the continuum state \mathbf{k}_{bx} (the ground state has $E < 0$) and

$$U_{\alpha; \alpha'} = \langle \phi_\alpha(\mathbf{r}) | V_{bA}(\mathbf{r}_b) + V_{xA}(\mathbf{r}_x) | \phi_{\alpha'}(\mathbf{r}) \rangle, \quad (8)$$

where $V_{xA}(\mathbf{r}_x)$ and $V_{bA}(\mathbf{r}_b)$ are the total (nuclear and Coulomb) interactions between $x - A$ and $b - A$ systems respectively. In Eq. (8) integrations are done over \mathbf{r} . In the DWBA f_α is obtained by solving Eq. (7) with only the diagonal $U_{\alpha; \alpha}$ and coupling from ground-state $U_{\alpha; 0}$ potentials. This enables each f_α to be obtained independently of the others.

2.3 Projectile states

The projectile state (J_p, \mathbf{k}_{bx}) is composed of a core of spin I and a valence nucleon of spin s in angular momentum state(s) lj , according to the general fractional parentage expansion

$$\phi_{J_p \mu_p, \mathbf{k}}(\mathbf{r}) = \sum_{\ell j I} A_{\ell s j}^{j I J} [\phi_I \varphi_{\ell s j, k}(\mathbf{r})]_{J_p \mu_p}. \quad (9)$$

where $A_{\ell s j}^{j I J}$ are the coefficients of the fractional parentage. The radial part of the single-particle states $\varphi_{\ell s j, k}$ is defined as $u_{\ell s j, k}(r)$.

In order to describe the breakup of a projectile such as ${}^8\text{B}$, we consider the inelastic excitations in the $p+{}^7\text{Be}$ system from the ground state $\phi_0(r)$ to excited states $u_{\ell s j, k}(r)$ in the continuum corresponding to momentum k and partial wave ℓ . The use of such single energy eigenstates, however, will result in calculation of the inelastic form factors which will not converge, as the continuum wave functions do not decay to zero as $r \rightarrow \infty$ sufficiently fast to have square norms. One way [16, 17] of dealing with this divergence is to take continuum states not

at a single energy, but averaged over a narrow range of energies. The resulting ‘bin’ states, which *are* square integrable, are defined as

$$u_{\ell sj, \{k_1, k_2\}}(r) = \sqrt{\frac{2}{\pi N}} \int_{k_1}^{k_2} w(k) e^{-i\delta_k} u_{\ell sj, k}(r) dk \quad (10)$$

with δ_k the scattering phase shift for $u_{\ell sj, k}(r)$, and with $N = \int_{k_1}^{k_2} |w(k)|^2 dk$ for some weight function $w(k)$ usually unity. The bin states are normalized as $\langle u|u \rangle = 1$ provided a sufficiently large maximum radius R_m for r is taken. They are orthogonal to any bound state, and also to other bin states if their energy ranges do not overlap. This construction can be easily generalized to give coupled-channels bin wave functions.

The rms radius of a bin wave function increases as the bin width $k_2 - k_1$ decreases, approximately as $1/(k_2 - k_1)$, so large radial ranges are needed to use the narrow bin states accurately. If the maximum radius R_m is not sufficiently large, then the wave functions $u(r)$ will not be normalized to unity by the factors given in equation (10). It is important however, to realize that the missing normalization comes from large distances; the bin wave functions must not be artificially renormalized to unity, otherwise, for example, the correct Coulomb $B(E\lambda)$ distributions will not be obtained.

2.4 Breakup couplings

As discussed above, the couplings $U_{\alpha: \alpha'}(R)$ in Eq. (7) arise from the interaction potentials of the projectile fragments with respect to the target. We first define a coupling X for the spatial parts ℓL of the motion by means of the single-folding integral

$$X_{\ell \mathbf{k} L: \ell' \mathbf{k}' L'}^\Lambda(R) = \langle (\ell L) \Lambda, \mathbf{k} | V_{bA}(\mathbf{r}_b) + V_{xA}(\mathbf{r}_x) | (\ell' L') \Lambda, \mathbf{k}' \rangle \quad (11)$$

Assuming that the potentials V_{bA} and V_{xA} contain only scalar components, the R - and r -dependent Legendre multipole potentials can be formed as

$$\mathcal{V}_\lambda(R, r) = \frac{1}{2} \int_{-1}^{+1} [V_{bA}(\mathbf{r}_b) + V_{xA}(\mathbf{r}_x)] P_\lambda(u) du \quad (12)$$

where K is the multipole moment and $u = \hat{\mathbf{r}} \cdot \hat{\mathbf{R}}$ is the cosine of the angle between \mathbf{r} and \mathbf{R} . The coupling form factor between states $u_{\ell \mathbf{k}}(r)$ and $u_{\ell' \mathbf{k}'}(r)$ is then

$$\begin{aligned} X_{\ell \mathbf{k} L: \ell' \mathbf{k}' L'}^\Lambda(R) &= \frac{1}{2} \sum_\lambda \int_0^{R_m} u_{\ell \mathbf{k}}(r) \mathcal{V}_\lambda(R, r) u_{\ell' \mathbf{k}'}(r) dr \quad (-1)^{\Lambda+\lambda} \hat{\ell} \hat{L} \hat{\ell}' \hat{L}' \\ &\times (2K+1) W(\ell \ell' L L'; \lambda \Lambda) \begin{pmatrix} \lambda & \ell & \ell' \\ 0 & 0 & 0 \end{pmatrix} \begin{pmatrix} \lambda & L & L' \\ 0 & 0 & 0 \end{pmatrix} \quad (13) \end{aligned}$$

Since I is the (fixed) spin of the core which is a spectator, the coupling in the full set of equations (7) is

$$\begin{aligned}
U_{\alpha:\alpha'}(R) &= \sum_{F\Lambda I j j' \ell \ell'} \hat{j} \hat{j}' (2F+1) \hat{J}_p \hat{J}_p (2\Lambda+1) W(\ell s J_p I; j F) W(\ell' s J_p I; j' F) \\
&\times A_{\ell' s j'}^{j' I J_p} A_{\ell s j}^{j I J_p} W(L \ell J F; \Lambda J_p) W(L' \ell' J F; \Lambda J_p) X_{\ell L: \ell' L'}^\Lambda(R) \quad (14)
\end{aligned}$$

3 The numerical procedure and application to ^8B breakup

The radial wave function in Eq. (6) is written asymptotically as

$$f_{L_f, J_p \mathbf{k}_{bx}}^{J_f}(R) \rightarrow \left(\frac{k_a}{k_{bx}}\right)^{1/2} (\Delta k_{bx})^{1/2} S_{L_f}^{J_f}(k_{bx}) H_{L_f}^{(+)}(k_{bx} r), \quad (15)$$

where k_a is the wave number in the entrance channel, Δk_{bx} is the bin width, and $H_{L_f}^{(+)}(\rho)$ is the Coulomb-modified outgoing wave. The S-matrix elements S_{L_f} can be obtained numerically as the asymptotic coefficients of analytic Coulomb wave functions fitted to the numerical solutions of f_α at $r = 50 \text{ fm}$.

Breakup cross sections can be computed from the S-matrix elements defined above or from the equation

$$T_{DWBA}^{(-)} = \langle \Psi_{J_f}^{M_f(-)}(\mathbf{R}, \mathbf{r}) | V_{bA}(\mathbf{r}_b) + V_{xA}(\mathbf{r}_x) | \phi_0(\mathbf{r}) \chi_{aA}^{(+)}(\mathbf{K}_i, \mathbf{R}) \rangle. \quad (16)$$

In this equation ϕ_0 is the ground state wave function of the projectile whereas $\chi_{aA}^{(+)}(\mathbf{K}_i, \mathbf{R})$ describes the relative motion of the projectile with respect to the target. The superscripts (+) and (-) specify the outgoing or incoming wave boundary conditions satisfied by the corresponding wave functions respectively. In this work the S-matrix method has been used.

The ^8B nucleus has a 2^+ ground state at -0.137 MeV , which is composed predominantly of the ^7Be core in its $3/2^-$ ground state and a valence proton in a $p_{3/2}$ configuration. $E1$ ($\lambda=1$) and $E2$ ($\lambda=2$) mechanisms will populate the ($s_{1/2}$, $d_{3/2}$, $d_{5/2}$) and ($p_{1/2}$, $p_{3/2}$, $f_{5/2}$, $f_{7/2}$) single particle continuum states respectively in the first step. We consider the excitation to states of these partial waves up to $E_{p-^7\text{Be}} = 3 \text{ MeV}$.

We have taken a single particle model for the structure of ^8B assuming that all states in ^8B are determined by the g.s. potential defined in [19]. This simplification of the $^7\text{Be}-p$ scattering state interaction, neglecting the core couplings and the M1 transitions, has hardly any effect on the integrated CD cross section ([12]) at non-relativistic energies.

As remarked earlier, in the DWBA calculations we have to use diagonal channel potentials for the entrance and exit channels. Different choices for these potentials

are (a) pure ${}^8\text{B}$ +target Coulomb, (b) Coulomb + some fixed optical potential, or (c) using the monopole ($\lambda = 0$) parts of the single-folded potentials (eq. 11). Choice (a) is appropriate for comparison with simple (e.g. semiclassical) models. Choice (b) is inaccurate for breakup states, as can be seen by comparison with the very diffuse potentials found in method (c). Choice (c) has the advantage that it generalizes readily when all the diagonal/off-diagonal monopole/multipole couplings need to be calculated for a full CDCC calculation.

For the Notre Dame experiment on the Coulomb dissociation of ${}^8\text{B}$ on ${}^{58}\text{Ni}$ at 26 MeV [10], good accuracy for the continuum discretization is obtained if we use 13 bins per partial wave, defined in the following way: 9 bins of 100 keV centered at 0.15; 0.25; ...; 0.95 MeV and 4 bins of 500 keV centered at 1.25; 1.75; 2.25; 2.75 MeV. Sufficient convergence for the $E1$ and $E2$ transitions was obtained if the maximum number of the partial waves (l_{max}) and the maximum radius (R_{max}) were taken to be $600\hbar$ and 300 fm respectively. Coupled asymptotic wave functions [22] are used beyond 30 fm.

For the RIKEN experiment on the Coulomb dissociation of ${}^8\text{B}$ on ${}^{208}\text{Pb}$ at 415 MeV [9], good accuracy for the continuum discretization is obtained if we use 8 bins per partial wave, defined in the following way: 4 bins of 250 keV centered at 0.125; 0.375; 0.625; 0.875 MeV and 4 bins of 500 keV centered at 1.25; 1.75; 2.25; 2.75 MeV. The bin wave functions were each integrated with 200 k -steps, out to $R_m = 50$ fm. In order to obtain convergence for the $E1$ and $E2$ transitions in this case, we include up to $l_{max} = 10000\hbar$ and $R_{max} = 1000$ fm for the reaction mechanism. Coupled asymptotic wave functions [22] are used beyond 50 fm.

4 Results and discussion

In Figs. 1a and 1b, we show the angular distributions of ${}^7\text{Be}$ and ${}^8\text{B}^*$ respectively in a ${}^8\text{B}$ induced breakup reaction on ${}^{58}\text{Ni}$ target at the beam energy of 25.8 MeV. Pure Coulomb and pure nuclear breakup cross sections are represented by the dashed and dashed-dotted curves respectively. The cross sections obtained by summing coherently the Coulomb and nuclear amplitudes (to be referred as *total* in the following) are represented by the solid lines. In these calculations the procedure of single-folding the respective fragment-target interactions with ${}^8\text{B}$ ground and continuum state wave functions (Eq. (11)) have been used. Nuclear parts of p - ${}^{58}\text{Ni}$ and ${}^7\text{Be}$ - ${}^{58}\text{Ni}$ interactions have been taken from Refs. [23] and [24] respectively. The curves in Fig. 1b improve on those in [13] by the inclusion of f -wave final states.

The angular distributions of ${}^7\text{Be}$ and ${}^8\text{B}^*$ are distinctly different from each other. While pure Coulomb and *total* breakup cross sections show a forward peak in case of ${}^7\text{Be}$ (which is typical of the angular distribution of fragments emitted in breakup reactions), those of ${}^8\text{B}^*$ tend to zero as angle goes to zero. The latter

is the manifestation of the adiabatic cut-off typical of the Coulomb-excitation process. In both the cases the nuclear effects are small below 20° and there is a Coulomb-nuclear interference minimum between 25° - 60° . However the magnitude of various cross sections are smaller in Fig. 1a. Furthermore, the nuclear-dominated peak occurs at different angles in Figs 1a ($\simeq 55^\circ$) and 1b ($\simeq 70^\circ$). As discussed in section (2.1), the angles of ${}^7\text{Be}$ can be related to those of ${}^8\text{B}^*$. A given $\theta_{7\text{Be}}$ gets contributions from a range of generally larger $\theta_{8\text{B}^*}$. This explains to some extent the shifting of the peaks of various curves to lower angles in Fig. 1a as compared to the corresponding ones in Fig. 1b. This underlines the importance of three-body kinematics in describing the inclusive breakup reactions.

The ratio of the experimental integrated breakup cross section of ${}^7\text{Be}$ (obtained by integrating the breakup yields in the angular range, $(45 \pm 6)^\circ$, of the experimental setup) to Rutherford elastic scattering of ${}^8\text{B}$ is reported to be $(8.1 \pm 0.8_{-0.5}^{+2.0}) \times 10^{-3}$ [10]. It is not possible to get this cross section by directly integrating the angular distributions shown in Fig. 1b in this angular range as the corresponding angles belong to ${}^8\text{B}^*$ and not to ${}^7\text{Be}$. However, in the three-body case (Fig. 1a), this can be done in a straight-forward way. This gives a value of 7.0×10^{-3} which is in close agreement with the experimental data. Thus, previous failures to explain the experimental value may be attributed to the neglect of both the Coulomb-nuclear interference effects and the three-body kinematics.

In Fig. 2, we have investigated the range of the validity of the point-like projectile and target approximation (PLPTA) and the role of the Coulomb-nuclear interference effects on the cross sections of $E1$ and $E2$ components for the reaction discussed in Fig. 1a. In Fig. 2a the results for pure Coulomb breakup are shown. $E1$ and $E2$ components of the cross section obtained by the single-folding procedure are shown by solid and dashed lines respectively, while those obtained with the PLPTA by solid and dashed lines with solid circles. It can be noted that PLPTA is not valid for angles beyond 20° . The condition that the impact parameter of the collision is larger than the sum of the projectile and target radii ($b > R_p + R_T$), assumed in applying the Alder-Winther theory, is no longer valid because there is a long tail in the ${}^8\text{B}$ ground state wave function. We also note that the $E2$ component is affected more by the PLPTA as compared to $E1$. The big difference in the $E1$ and $E2$ cross sections seen in the PLPTA results beyond 20° (where $E2$ component is much bigger than the $E1$), almost disappears in the corresponding cross sections obtained by single-folding procedure. Nevertheless, the $E2$ cross sections still remain larger than those of the $E1$ beyond 30° in the latter case.

Dipole ($'E1'$) and quadrupole ($'E2'$) cross sections for pure nuclear breakup are shown in Fig. 2b while those for the *total* case are shown in Fig. 2c. We notice that the Coulomb-nuclear interference effects make the contributions of the $E1$ component larger than those of $E2$ at all the angles. This result is quite remarkable as it implies that the $E2$ component in the breakup of ${}^8\text{B}$ is not dominant even at the subCoulomb beam energies. Therefore, there is hardly any

hope of determining the $E2$ component of ${}^8\text{B}$ breakup by Notre Dame type of experiment [10].

This underlines the need for more refined experiments to determine the $E2$ component (as already pointed out in Ref. [8]). It is clear from Fig. 2c that the measurements of the angular distributions may provide useful information about the $E2$ component as it is different from that of the $E1$ multipolarity. On the other hand, the angular distributions of the fragments, calculated within a semiclassical theory without making the approximation of isotropic angular distributions in the projectile rest frame, have been shown to have large $E1 - E2$ interference effects [26, 27]. They lead to asymmetries in the momentum distributions of the fragments, whose measurements may enable one to put constraints on the $E2$ component [28]. However, for the better accuracy of this method, improved calculations including the nuclear effects are necessary.

Our results for the nuclear effects in the angular distribution of ${}^8\text{B}^*$ are approximately similar to that reported in [29], where Coulomb and nuclear form factors are calculated by folding the proton-target mean-field (parameterized by a Woods-Saxon function) by the ground and discretized continuum state ${}^8\text{B}$ wave functions. Those authors calculate various cross sections by integrating a fixed projectile-target optical potential along a semiclassical trajectory. However, since the three-body kinematics for the final state has not been considered by them, a direct comparison between their calculations and the data of [10] is not possible.

In Fig. 3a, we show $E1$ and $E2$ components of the angular distributions for the ${}^8\text{B} + {}^{208}\text{Pb} \rightarrow {}^8\text{B}^* + {}^{208}\text{Pb}$ reaction measured by the Kikuchi et al. [9] at the beam energy of 415 MeV, for the pure Coulomb excitation case. The dashed, dotted and solid lines represent $E1$, $E2$ and $E1 + E2$ cross sections respectively which are obtained by the single-folding procedure. Also shown in this figure are the corresponding results obtained by PLPTA (curves with solid circles). We note that PLPTA becomes inaccurate beyond 4° in this case. Moreover, the $E2$ component of the pure Coulomb excitation becomes increasingly important also after this angle.

In Fig. 3b, the *total* cross sections are shown. The nuclear part of the fragment-target interaction at these energies have been taken from [23] (for proton) and [25] (for ${}^7\text{Be}$). The dashed and dotted lines show the $E1$ and $E2$ cross sections respectively, while the solid line represents their sum. It can be noted that nuclear effects modify the pure Coulomb $E1$ cross sections substantially after $\sim 4^\circ$, and the $E2$ cross sections in the entire angular range. However, since the $E2$ components are quite small at angles $\leq 4^\circ$, the difference between pure Coulomb and *total* $E1 + E2$ cross sections is appreciable only after this angle.

Therefore, at RIKEN energies, the PLPTA breaks down beyond 4° , where the Coulomb-nuclear interference effects as well as the $E2$ component of breakup is substantial. Hence, the Coulomb dissociation method as used in e.g. Ref. [6] to

extract a reliable $S_{17}(0)$ from the measurements of the angular distributions in the breakup of ${}^8\text{B}$ on heavy target at RIKEN energies (~ 50 MeV/nucleon), is useful only when data is taken at angles below 4° .

In Figs. 4a, 4b and 4c we show the comparison of our calculations for $\epsilon \cdot d\sigma/d\theta$ with the experimental data of Kikuchi et al. [9] as a function of the scattering angle $\theta_{\delta_{B^*}}$ of the excited ${}^8\text{B}$ (center of mass of the ${}^7\text{Be}+p$ system) for three relative energy bins. We have used the efficiency (ϵ) matrix as well as angular and energy averaging as discussed in Ref. [9] which is provided to us by the RIKEN collaboration. The dashed and dotted lines are the pure Coulomb $E1+E2$ and $E2$ cross sections while the solid and dashed lines are the corresponding *total* cross sections. We note that our calculations are in fair agreement with the experimental data. We stress that no arbitrary normalization constant has been used in the results reported in this figure.

The $E2$ component of breakup is significant at almost all the angles in the relative energy bin 2.0 – 2.25 MeV(c), and at angles beyond 5° in the energy bin 1.25 – 1.50 MeV(b). On the other hand, its contribution is inconsequential in the energy bin 0.5 – 0.75 MeV (a). This result is in somewhat disagreement with that reported in Ref. [9], where this component is reported to be small everywhere below 1.75 MeV relative energy. Although these authors also perform a quantum mechanical calculation within DWBA, their treatment of the continuum state is very different from ours. Moreover they use a collective model prescription for the Coulomb and nuclear form factors, which has a limited applicability for ${}^8\text{B}$ breakup. Bertulani and Gai [30] have also reported smaller $E2$ component in their analysis of this data. These authors do not include the nuclear effects in the $E1$ excitations and make use of the eikonal approximation to calculate the $E2$ nuclear excitation amplitudes. Moreover, the Coulomb excitation amplitudes have been calculated with the PLPTA which we have found to be invalid at higher angles (see Fig. 3). It is also noted in Fig.3 that Coulomb-nuclear interference effects reduce the $E1$ cross sections at larger angles.

Some authors have pointed out the importance of the higher order effects in the Coulomb breakup of ${}^8\text{B}$, where $E1$ and $E2$ components interfere destructively [27, 31]. It should be remembered here that our results are based on a one-step distorted wave theory. It would be worthwhile to perform multistep calculations within a full quantum mechanical theory including the nuclear and Coulomb-nuclear interference effects (this has not been done so far) in order to study the effects of dynamical higher order processes for this reaction.

5 Summary and Conclusions

In this paper, we studied the breakup reactions ${}^8\text{B} + {}^{58}\text{Ni} \rightarrow {}^7\text{Be} + \text{X}$ and ${}^8\text{B} + {}^{208}\text{B} \rightarrow {}^8\text{B}^* + {}^{208}\text{Pb}$, at beam energies of 25.8 and 415 MeV respectively, within

the framework of the one-step prior-form distorted wave Born-approximation. In this theory, the breakup process is described as a single proton excitation of the projectile from its ground state to a range of states in the continuum, which is discretized by the method of continuum bins. In this method, both Coulomb and nuclear breakup as well as their interference terms are calculated within the same framework. Moreover, we use the three-body kinematics while calculating the cross sections for the ${}^7\text{Be}$ fragment in the first reaction.

For the breakup reaction at low energy the Coulomb-nuclear interference effects are found to be quite important. This leads to a reduction in the pure Coulomb dissociation cross sections for the ${}^7\text{Be}$ fragment in the angular range of the measurements reported in [10], which together with the three-body kinematics reproduces the experimental integrated cross section for this fragment. This agreement had eluded the pure Coulomb dissociation calculations.

A very striking feature of the Coulomb-nuclear interference effect is that it makes the $E1$ component larger than the $E2$ at all the angles, which renders untenable the main objective of the Notre Dame experiment of determining the $E2$ component in the breakup of ${}^8\text{B}$ at low beam energies. The dominance of the $E2$ component seen in the semi-classical Alder-Winther theory of Coulomb excitation has led to this expectation. However, we note that even in pure Coulomb dissociation process, with finite size of the projectile taken into account, the $E2$ components is almost equal to that of $E1$ in the relevant angular range.

The breakup data at higher beam energies (RIKEN energies), are almost free from the nuclear effects and are dominated by the $E1$ component for ${}^7\text{Be}$ - p relative energies < 0.75 MeV at very forward angles ($\leq 4^\circ$). The study of the breakup of ${}^8\text{B}$ in this kinematical regime is, therefore, better suited for the extraction of reliable $S_{17}(0)$ for the capture reaction ${}^7\text{Be}(p, \gamma){}^8\text{B}$ at low relative energies.

One of the authors (RS) would like to acknowledge an associateship award from the Abdus Salam International Centre of Theoretical Physics, Trieste. This work is supported by Engineering and Physical Sciences Research Council, UK, grant nos. J/95867 and L/94574.

References

- [1] G. Baur and H. Rebel, J.Phys.G:Nucl. and Part. Phys. **20**, 1 (1994)
- [2] G. Baur and H. Rebel, Ann. Rev. Nuc. Part. Sc. **46**, 321 (1997).
- [3] J.N. Bahcall, Neutrino Astrophysics, Cambridge University Press, New York, 1989; J.N. Bahcall, M.H. Pinsonneault, Rev. Mod. Phys. **67**, 781 (1995); J.N. Bahcall, Nucl. Phys.A **631**, 29 (1998).
- [4] S. Turck-Chieze et al., Phys. Rep. **230**, 57 (1993).
- [5] T. Motobayashi et al., Phys. Rev. Letts. **73**, 2680 (1994).

- [6] R. Shyam, I.J. Thompson and A.K. Dutt-Majumder, Phys. Lett.B **371**,1 (1996).
- [7] K. Alder and A. Winther, *Electromagnetic Excitation*, (North Holland, Amsterdam, 1975).
- [8] K. Langanke, T.D. Shoppa, Phys. Rev.C **49**, R1771 (1994); **51** (1995) 2844(E); **52** (1995) 1709.
- [9] T. Kikuchi et al., Phys. Letts. **B391**, 261 (1997).
- [10] Johannes von Schwarzenberg et al., Phys. Rev. **C53**, R2598 (1996).
- [11] R. Shyam and I.J. Thompson, Phys. Lett.B **415**, 315 (1997).
- [12] F.M. Nunes, R. Shyam and I.J. Thompson, J.Phys.G **24**, 1575 (1998).
- [13] F.M. Nunes and I.J. Thompson, Phys. Rev.C **57**, R2818(1998)
- [14] G. Baur and M. Weber, Nucl. Phys. A **504**, 352 (1989); H. Esbensen and G. Bertsch, Phys. Lett.B **359**, 13 (1995).
- [15] H. Fuchs, Nucl. Instr. & Methods **200**, 361 (1982); C.A. Bertulani, Phys. Rev. C **49**, 2688 (1994).
- [16] G.H. Rawitscher, Phys. Rev. **C9**, 2210 (1974), **C11**, 1152 (1975), Nucl. Phys. **A241**, 365 (1975); M. Yahiro and M. Kamimura, Prog. Theor. Phys. **65**, 2046 (1981), **65**, 2051 (1981).
- [17] Y. Sakuragi, M. Yahiro and M. Kamimura, Prog. Theor. Phys. Suppl. **89**, 136 (1986).
- [18] K.H. Kim, M.H. Park and B.T. Kim, Phys. Rev.C **53**, 363 (1987).
- [19] H. Esbensen and G. Bertsch, Nucl. Phys.A **600**, 37 (1996).
- [20] Y. Hirabayashi and Y. Sakuragi, Phys. Rev. Lett. **69**, 1892 (1992).
- [21] I.J. Thompson, Computer Physics Reports, **7**, 167 (1988).
- [22] J. Christley and I.J. Thompson, Comp. Phys. Comm., **79**, 143 (1994).
- [23] F.D. Becchetti and G.W. Greenlees, Phys. Rev. **182**, 1190 (1969).
- [24] C.W. Glover, R.I. Cutler and K.W. Kemper, Nucl. Phys.A **341**, 137 (1980).
- [25] A.F. Zeller, D.C. Weissner, T.R. Ophel and D.F. Hebbard, Nucl. Phys.A **332**, 515 (1979).
- [26] H. Esbensen and G.F. Bertsch, Phys. Lett.B **359**, 13(1995).
- [27] H. Esbensen and G.F. Bertsch, Nucl. Phys.A **600**, 66 (1996)
- [28] B. Davids et al., Preprint NSUCL-1095 (Michigan State University, March 1998).
- [29] C.H. Dasso, S.M. Lenzi and A. Vitturi, Nucl. Phys. A. (in press)
- [30] C.A. Bertulani and M. Gai, Nucl. Phys. A **636**, 227 (1998).
- [31] S. Typel, H. Wolter and G. Baur, Nucl. Phys.A **617**, 147 (1997).

Figure Captions

- Fig. 1 Angular distribution of the ${}^7\text{Be}$ fragment emitted in the breakup reaction of ${}^8\text{B}$ on ${}^{58}\text{Ni}$ target at the beam energy of 25.8 MeV. The dashed and dashed-dotted lines show the pure Coulomb and pure nuclear breakup cross sections respectively while their coherent sum is represented by the solid line. (b) Angular distribution of ${}^8\text{B}^*$ in the Coulomb excitation of ${}^8\text{B}$ on ${}^{58}\text{Ni}$ at the beam energy of 25.8 MeV. The dashed and dashed-dotted lines show the cross sections for pure Coulomb and pure nuclear excitation respectively, while the solid line represents their coherent sum.
- Fig. 2 Dipole (solid lines) and quadrupole (dashed lines) components of the angular distributions of the ${}^7\text{Be}$ fragment emitted in the breakup reaction of ${}^8\text{B}$ on ${}^{58}\text{Ni}$ target at the beam energy of 25.8 MeV. (a) pure Coulomb breakup; also shown here are the $E1$ (solid lines with solid circles) and $E2$ (dashed lines with solid circles) cross sections obtained with point-like projectile and target approximation (Alder-Winther theory), (b) pure nuclear breakup and (c) Coulomb plus nuclear breakup where the corresponding amplitudes are coherently summed.
- Fig. 3 Angular distribution for ${}^8\text{B}+{}^{208}\text{Pb} \rightarrow {}^8\text{B}^*({}^7\text{Be}+p)+{}^{208}\text{Pb}$ reaction at the beam energy of 415 MeV. (a) Results for pure Coulomb excitation, the dashed and dotted curves represent the $E1$ and $E2$ cross sections while their sum is depicted by the solid line. Also shown here are the results obtained with a point-like projectile and target approximation (Alder-Winther theory), where dashed and dotted lines with solid circles show the corresponding $E1$ and $E2$ cross sections while the solid line with solid circles represents their sum. (b) Coherent sum of Coulomb and Nuclear excitation calculations; the dashed and dotted lines show the $E1$ and $E2$ components while the solid line is their sum.
- Fig. 4 Comparison of experimental and theoretical cross section $\epsilon d\sigma/d\theta$ as a function of the scattering angle $\theta_{8\text{B}^*}$ for three relative energy bins of (a) 500-750 keV, (b) 1250-1500 keV, (c) 2000-2250 keV. ϵ is the detector efficiency. Solid lines show the calculated $(E1+E2)$ Coulomb plus nuclear dissociation cross sections while the dashed lines represents the corresponding pure Coulomb dissociation result. Pure $E2$ Coulomb and Coulomb+nuclear cross sections are shown by dotted and dashed-dotted lines. The experimental data and the detector efficiencies are taken from [9].

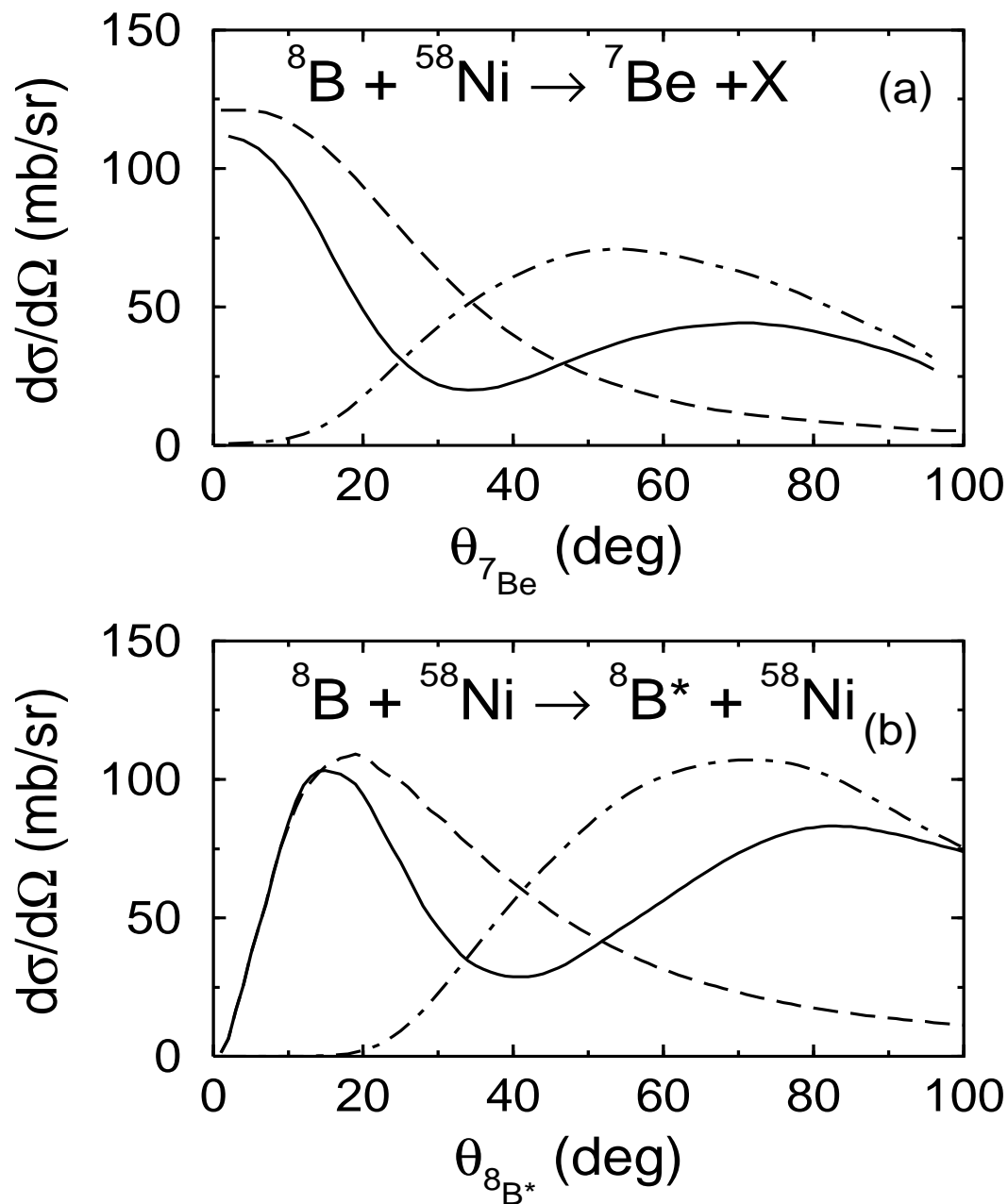


Figure 1: (a) Angular distribution of the ${}^7\text{Be}$ fragment emitted in the breakup reaction of ${}^8\text{B}$ on ${}^{58}\text{Ni}$ target at the beam energy of 25.8 MeV. The dashed and dashed-dotted lines show the pure Coulomb and pure nuclear breakup cross sections respectively while their coherent sum is represented by the solid line. (b) Angular distribution of ${}^8\text{B}^*$ in the Coulomb excitation of ${}^8\text{B}$ on ${}^{58}\text{Ni}$ at the beam energy of 25.8 MeV. The dashed and dashed-dotted lines show the cross sections for pure Coulomb and pure nuclear excitation respectively, while the solid line represents their coherent sum.

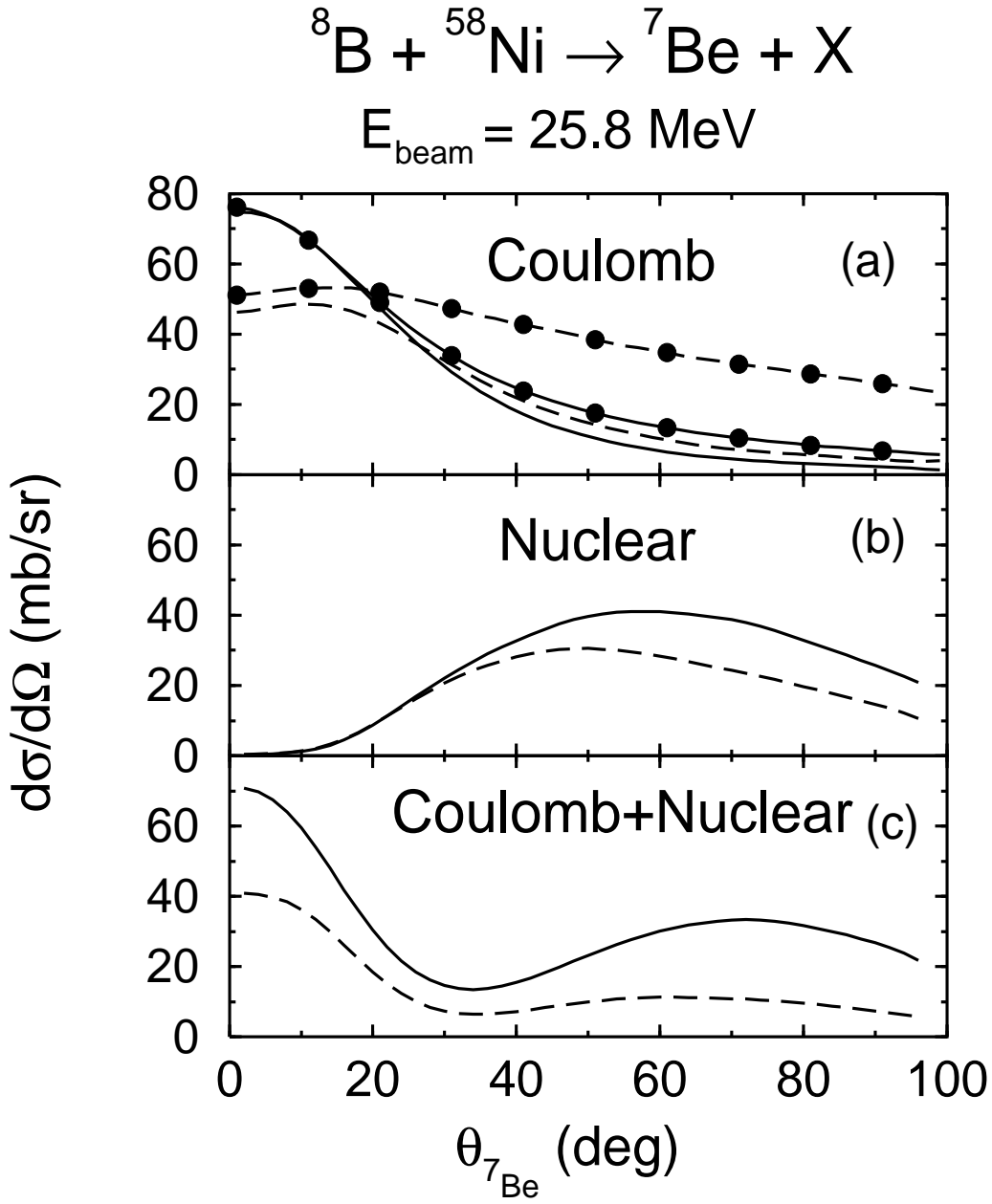


Figure 2: Dipole (solid lines) and quadrupole (dashed lines) components of the angular distributions of the ${}^7\text{Be}$ fragment emitted in the breakup reaction of ${}^8\text{B}$ on ${}^{58}\text{Ni}$ target at the beam energy of 25.8 MeV. (a) pure Coulomb breakup; also shown here are the $E1$ (solid lines with solid circles) and $E2$ (dashed lines with solid circles) cross sections obtained with point-like projectile and target approximation (Alder-Winther theory), (b) pure nuclear breakup and (c) Coulomb plus nuclear breakup where the corresponding amplitudes are coherently summed.

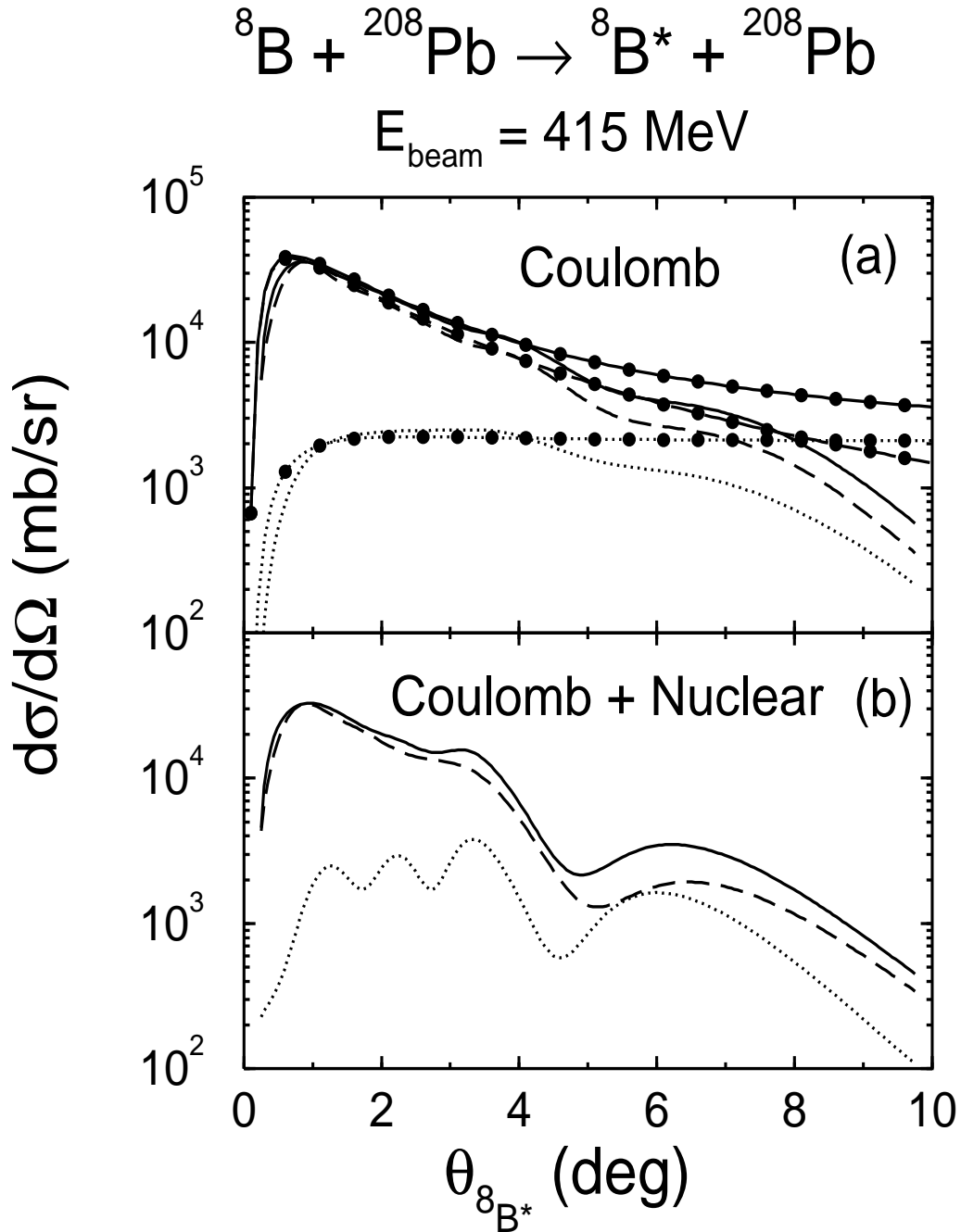


Figure 3: Angular distribution for ${}^8\text{B} + {}^{208}\text{Pb} \rightarrow {}^8\text{B}^*({}^7\text{Be} + \text{p}) + {}^{208}\text{Pb}$ reaction at the beam energy of 415 MeV. (a) Results for pure Coulomb excitation, the dashed and dotted curves represent the $E1$ and $E2$ cross sections while their sum is depicted by the solid line. Also shown here are the results obtained with a point-like projectile and target approximation (Alder-Winther theory), where dashed and dotted lines with solid circles show the corresponding $E1$ and $E2$ cross sections while the solid line with solid circles represents their sum. (b) Coherent sum of Coulomb and Nuclear excitation calculations; the dashed and dotted lines show the $E1$ and $E2$ components while the solid line is their sum.

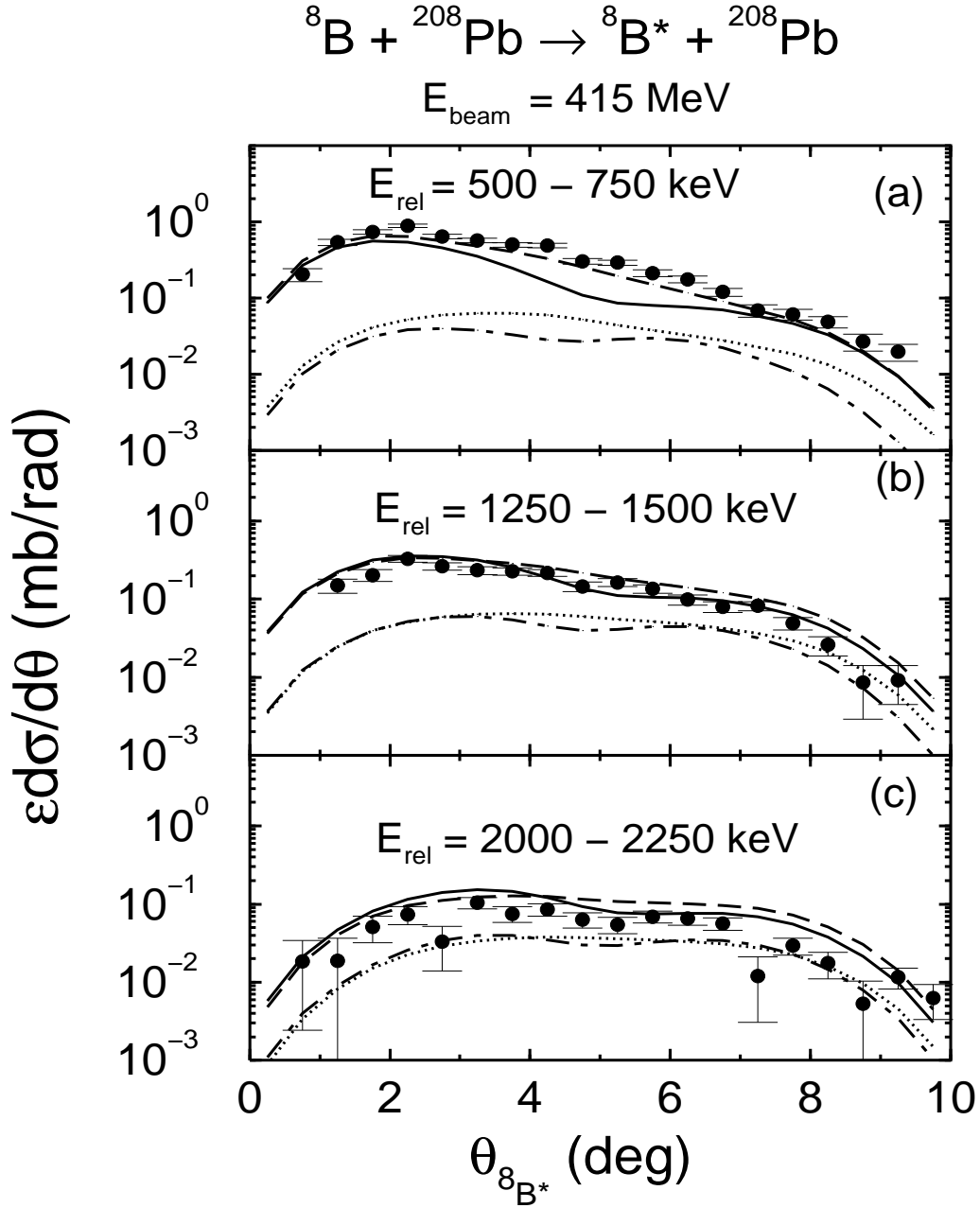


Figure 4: Comparison of experimental and theoretical cross section $\epsilon d\sigma/d\theta$ as a function of the scattering angle $\theta_{8\text{B}^*}$ for three relative energy bins of (a) 500-750 keV, (b) 1250-1500 keV, (c) 2000-2250 keV. ϵ is the detector efficiency. Solid lines show the calculated $(E1 + E2)$ Coulomb plus nuclear dissociation cross sections while the dashed lines represents the corresponding pure Coulomb dissociation result. Pure $E2$ Coulomb and Coulomb+nuclear cross sections are shown by dotted and dashed-dotted lines. The experimental data and the detector efficiencies are taken from [9].